ELSEVIER

Surface Science 444 (2000) 221–235

surface science

www.elsevier.nl/locate/susc

Atomic linewidths and line shifts near a dielectric layer, and the limit of a semi-infinite medium

Henk F. Arnoldus *

Department of Physics and Astronomy, Mississippi State University, P.O. Drawer 5167, Mississippi State, MS 3762-5167, USA

Received 26 January 1999; accepted for publication 9 September 1999

Abstract

The linewidth and line shift of an atom near a dielectric medium have been studied. The effect of the presence of the material is either a line narrowing or a line broadening, as compared to the natural linewidth, and it appears that the general tendency is a line narrowing. The corresponding shift is predominantly towards the blue. We illustrate graphically that the theoretical limit of a perfect conducting metal is unrealistic for any existing material, in particular when the atomic dipole is oriented perpendicular to the surface. We show that the limit of a semi-infinite medium follows from a delicate average over fast oscillations, and that the result is different from what one would expect. Explicit expressions for the linewidth were obtained for the case where the atom is close to the surface.

Keywords: Atom–solid interactions; Dielectric phenomena; Metallic surfaces; Quantum effects

1. Introduction

Optical properties of an atom are determined not only by its internal Hamiltonian, but also by its environment, a prediction first made by Purcell [1]. Already the finite lifetime of an excited electronic state is a consequence of the coupling between the atomic dipole moment and the electromagnetic field of the embedding vacuum [2]. For a two-state atom with excited level $|e\rangle$ and ground level $|g\rangle$, separated by an energy of $\hbar\omega_o$, the Einstein A coefficient for spontaneous decay is given by [3]

$$A_o = \frac{\omega_o^3}{3\pi\epsilon_o\hbar c^3}\boldsymbol{\mu}_{eg}\cdot\boldsymbol{\mu}_{eg}^*, \tag{1}$$

with $\boldsymbol{\mu}_{eg}=\langle e|\boldsymbol{\mu}|g\rangle$, the dipole moment matrix element between the two levels. The lifetime of level $|e\rangle$ is then $1/A_o$, and during a transition from $|e\rangle$ to $|g\rangle$ a fluorescent photon is emitted. When the atom is in the vicinity of material, the structure of the vacuum surrounding the atom changes, and this alters the value of this Einstein A coefficient. The first observation of the effect of media on the lifetime of a molecular excited electronic state was reported by Drexhage [4], who studied dye molecules on a dielectric substrate, and similar experiments were reported later [5–8]. For atoms in a microwave cavity, both inhibition and enhancement of spontaneous emission rates have been observed [9–11], and also in the optical domain it has been experimentally confirmed that the presence of media affects the emission rate [12–14]. In the most simple theoretical model, the medium is assumed to be a mirror (perfectly conducting

* Tel.: +1-662-325-2919. fax: +1-662-325-8898.
E-mail address: arnoldus@ra.msstate.edu (H.F. Arnoldus)

0039-6028/00/$ - see front matter
PII: S0039-6028(99)00996-6

metal) or a set of parallel mirrors [15–17]. Other approaches include the semiclassical energy transfer method [18,19], Green's function technique [20], and a linear response formalism [21–23].

Rather than measuring the decay rate of the excited atomic state (or equivalently, the emission rate of photons), one can also obtain the Einstein A coefficient by measuring the line shape for absorption of weak radiation [24]. The normalized absorption profile as a function of the angular frequency ω is given by

$$I(\omega)=\frac{1}{\pi}\,\mathrm{Re}\,\frac{1}{(1/2)A-i(\omega-\omega_0-\Delta)}, \tag{2}$$

a Lorentzian with a full width at half maximum equal to A. Although this linewidth is a consequence of the decay of the coherence between the two levels, instead of the decay of the population of the excited state, it reveals the same Einstein A coefficient, and thus the influence of the environment on the atom. The line is centered around $\omega=\omega_0+\Delta$, indicating a shift Δ away from resonance. For an atom in free space, $A=A_0$ and the shift $\Delta=\Delta_0$ is the Lamb shift [25]. Due to the vacuum and possible media, each atomic level will shift by a certain amount, and with a contribution from every other level. The total shift Δ is then the difference between the shift of $|e\rangle$ and the shift of $|g\rangle$. In our model two-state atom, the shift of $|e\rangle$ is only paired to $|g\rangle$, and vice versa, but in realistic calculations one has to sum over all pairs of levels, including the continuum. The effect of media on this shift has been studied theoretically with the same variety of approaches as the Einstein A coefficient [26–31]. Most theories for the lifetime yield the same result, but the expressions for the level shifts vary. In particular, semi-classical calculations seem to contradict quantum mechanical results.

Many models deal with an atom near a perfect conductor or in between parallel mirrors, or near a semi-infinite dielectric medium. This can be generalized to the situation of the case of an atom near a dielectric slab, which then includes the mirror as a special limit. In the present paper, we study the transition from a finite thickness material to the limit of a semi-infinite medium, using an approach based on Fresnel reflection and transmission coefficients. It appears that the limit of a semi-infinite medium does not simply follow from including some small absorption on the dielectric material, as one does in classical optics. Rather, the limit is reached by an effective average over fast oscillations. We have also obtained closed-form analytical solutions for the case where the atom is close to the surface, as compared to an optical wavelength. These explicit expressions are given in Appendix A.

2. Dipole interaction

An atom is located on the z-axis, a distance h above a layer of material of thickness L. The schematic setup is shown in Fig. 1. The medium is characterized by its dielectric constant ϵ. For $\epsilon>1$ we have a common dielectric, and for $\epsilon<0$ this reasonably models a metal, at least in the visible region of the spectrum. The atom interacts with electromagnetic radiation through the dipole interaction. With $\boldsymbol{E}(\boldsymbol{r}_0)$ the electric field at the location of the atom ($\boldsymbol{r}_0=h\boldsymbol{e}_z$), the interaction Hamiltonian is usually taken as

$$H_{\mathrm{ar}}=-\boldsymbol{\mu}\cdot\boldsymbol{E}(\boldsymbol{r}_0). \tag{3}$$

For the calculation of lifetimes this approximation yields the correct results, but for the level shift we

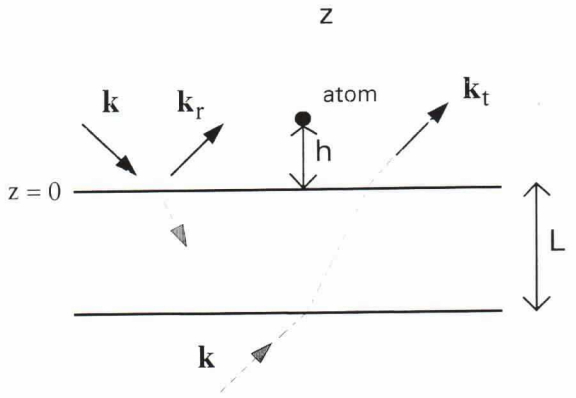

Fig. 1. Schematic illustration of the setup of the dielectric layer and the atom. Also shown are the wave vectors corresponding to the plane wave modes that determine the structure of the radiation field in the region $z>0$.

need the exact interaction Hamiltonian in Coulomb gauge [32]:

$$H_{\rm ar} = -\boldsymbol{M}\cdot\boldsymbol{A}(\boldsymbol{r}_{\rm o}). \tag{4}$$

Here, $\boldsymbol{A}$ is the vector potential, and the atomic operator $\boldsymbol{M}$ is defined as

$$\boldsymbol{M} = \sum_{\alpha}\frac{q_\alpha}{m_\alpha}\boldsymbol{p}_\alpha, \tag{5}$$

with q_α, m_α and $\boldsymbol{p}_\alpha$ the charge, mass and canonical momentum, respectively, of particle α inside the atom. The transition matrix elements of $\boldsymbol{M}$ are related to the dipole moment matrix elements according to [33]

$$\langle {\rm e}|\boldsymbol{M}|g\rangle = i\omega_{\rm o}\boldsymbol{\mu}_{\rm eg}. \tag{6}$$

3. Mode structure

Since no external fields are considered, the only radiation comes from the vacuum field. In empty space, the $\boldsymbol{E}$ field operator in the Heisenberg picture is given by

$$\boldsymbol{E}(\boldsymbol{r},t) = i\sum_{k\sigma}\sqrt{\frac{\hbar\omega}{2\epsilon_o V}}a_{k\sigma}\boldsymbol{e}_{k\sigma}\,{\rm e}^{i(\boldsymbol{k}\cdot\boldsymbol{r}-\omega t)} + {\rm H.c.}, \tag{7}$$

with $\boldsymbol{k}$, σ the transverse modes supported by the quantization volume V, $a_{k\sigma}$ the photon annihilation operators, $\boldsymbol{e}_{k\sigma}$ unit polarization vectors, and $\omega = ck$. Similar expressions hold for the magnetic field $\boldsymbol{B}$ and the vector potential. When incident on the medium, these plane waves partially reflect at the surface and partially travel into the material (see Fig. 1). In the field given by Eq. (7), waves propagate in all directions, and this implies that there are vacuum waves that are incident from the region $z<-L$. These waves travel through the layer and contribute to the field in $z>0$ where the atom is located. Consequently, in addition to the vacuum field from Eq. (7) there is now also a reflected (r) field and a transmitted (t) field. This t-waves field, with its origin in the vacuum field below the medium, is sometimes called 'quantum noise' [34,35].

The electromagnetic field operators ($\boldsymbol{E}$, $\boldsymbol{B}$ and $\boldsymbol{A}$) in the Heisenberg picture satisfy the classical Maxwell equations [36], including boundary conditions. With the incident field given by Eq. (7), this determines uniquely the solution in all space. For the vector potential in $z>0$ we then have

$$\begin{aligned}\boldsymbol{A}(\boldsymbol{r},t) = &\sum_{k\sigma}{}'' \sqrt{\frac{\hbar}{2\epsilon_{\rm o}\omega V}}a_{k\sigma}\boldsymbol{e}_{k\sigma}\,{\rm e}^{i(\boldsymbol{k}\cdot\boldsymbol{r}-\omega t)}\\ &+\sum_{k\sigma}{}'' \sqrt{\frac{\hbar}{2\epsilon_{\rm o}\omega V}}a_{k\sigma}\boldsymbol{e}_{k_r\sigma}R_{k\sigma}\,{\rm e}^{i(\boldsymbol{k}_r\cdot\boldsymbol{r}-\omega t)}\\ &+\sum_{k\sigma}{}' \sqrt{\frac{\hbar}{2\epsilon_{\rm o}\omega V}}a_{k\sigma}\boldsymbol{e}_{k_t\sigma}T_{k\sigma}\,{\rm e}^{i(\boldsymbol{k}\cdot\boldsymbol{r}-\omega t)} + {\rm H.c.}\end{aligned} \tag{8}$$

The double prime on the summation sign indicates that the sum only runs over waves coming in from $z>0$, whereas the single prime restricts the summation to waves incident from $z<-L$. The amplitude factors R_{ks} and T_{ks} are the Fresnel reflection and transmission coefficients for this geometry, which will be discussed in more detail in the next section. If we indicate by $\boldsymbol{k}_\parallel$ the parallel component of the incident wave vector $\boldsymbol{k}$ with respect to the surface $z=0$, and if we write u for the cosine of the angle of incidence, then we have for waves incident from above

$$\boldsymbol{k} = \boldsymbol{k}_\parallel - ku\boldsymbol{e}_z, \tag{9}$$

$$\boldsymbol{k}_r = \boldsymbol{k}_\parallel + ku\boldsymbol{e}_z. \tag{10}$$

For s-polarization we take the unit polarization vectors as

$$\boldsymbol{e}_{k_{(r)}s} = \frac{1}{k_\parallel}\boldsymbol{k}_\parallel\times\boldsymbol{e}_z, \tag{11}$$

and as phase convention for p-polarization we take

$$\boldsymbol{e}_{k_{(r)}p} = \frac{1}{k}\boldsymbol{k}_{(r)}\times\boldsymbol{e}_{k_{(r)}s}. \tag{12}$$

For waves incident from below we simply have $\boldsymbol{k}_t = \boldsymbol{k}$ and for the polarization vectors we take $\boldsymbol{e}_{k_t\sigma} = \boldsymbol{e}_{k\sigma}$.

4. Fresnel coefficients

With Eq. (7) for the incident field, and a corresponding expression for the magnetic field,

the boundary conditions at the two interfaces $z=0$ and $z=-L$ determine eight Fresnel coefficients for the various waves, given the $\boldsymbol{k}$ vector of the incident field. Since we are not concerned with the field inside the medium, we consider only R and T, both for s- and p-polarization. For simplicity of notation, we shall drop the subscript $\boldsymbol{k}$ on these coefficients. Explicitly, we have [37,38]

$$R_s=(1-\epsilon)\frac{1-\mathrm{e}^{2i\ell v}}{(v+u)^2-(v-u)^2\,\mathrm{e}^{2i\ell v}}, \tag{13}$$

$$R_p=[(u\epsilon)^2-v^2]\frac{1-\mathrm{e}^{2i\ell v}}{(v+u\epsilon)^2-(v-u\epsilon)^2\,\mathrm{e}^{2i\ell v}}, \tag{14}$$

$$T_s=\frac{4uv}{(v+u)^2-(v-u)^2\,\mathrm{e}^{2i\ell v}}\,\mathrm{e}^{i\ell(v-u)}, \tag{15}$$

$$T_p=\frac{4uv\epsilon}{(v+u\epsilon)^2-(v-u\epsilon)^2\,\mathrm{e}^{2i\ell v}}\,\mathrm{e}^{i\ell(v-u)}. \tag{16}$$

Here we have introduced the dimensionless layer thickness

$$\ell=kL=\frac{\omega L}{c}, \tag{17}$$

and the abbreviation

$$v=\sqrt{\epsilon-1+u^2}. \tag{18}$$

The z-components of the wave vectors for the field in the medium are $\pm kv$. For $\epsilon-1+u^2>0$ this v is positive, and it reflects that the waves in the medium are travelling waves. On the other hand, for $\epsilon-1+u^2<0$ the waves in the layer are evanescent, and v is positive imaginary. For $\epsilon>1$, this happens when the angle of incidence is larger than the critical angle. For ϵ negative, e.g. for metals, v is always imaginary (because $0\le u\le 1$).

The expressions for the Fresnel coefficients above hold for arbitrary complex ϵ. An imaginary part of ϵ (with $\mathrm{Im}\,\epsilon>0$) accounts for absorption in the material. Loss of energy in the medium would be in conflict with quantum mechanics in which the radiation field is represented by a Hamiltonian (as below). It can be shown that an imaginary part of ϵ would lead to contradictions, so we shall assume that ϵ is real. From the expressions above it can then be verified that the identity

$$|R_\sigma|^2+|T_\sigma|^2=1, \tag{19}$$

with $\sigma=s$ or p, holds. This relation will be important later on, and it should be noted that it only holds for real ϵ (or, v real or pure imaginary).

5. Master equation

Eq. (8) gives the vector potential in the Heisenberg picture. The Schrödinger representation follows from setting $t=0$, and if we then take $\boldsymbol{r}=h\boldsymbol{e}_z$ we have the field at the position of the atom. Then Eqs. (4) and (5) determine the interaction Hamiltonian between the radiation field and the atom. The Hamiltonian of the radiation is the usual one,

$$H_\mathrm{r}=\sum_{k\sigma}\hbar\omega\left(a^\dagger_{k\sigma}a_{k\sigma}+\frac{1}{2}\right), \tag{20}$$

although we do not need this for what is to follow. It simply determines the time evolution of the vector potential, which has already been given by Eq. (8). The internal Hamiltonian of the two-state atom is

$$H_\mathrm{a}=|\mathrm{e}\rangle\hbar\omega_\mathrm{e}\langle\mathrm{e}|+|\mathrm{g}\rangle\hbar\omega_\mathrm{g}\langle\mathrm{g}|, \tag{21}$$

with $\omega_\mathrm{e}-\omega_\mathrm{g}=\omega_\mathrm{o}$. The equation of motion for the density operator $\rho(t)$ of the entire system is then

$$i\hbar\frac{\mathrm{d}\rho}{\mathrm{d}t}=[H_\mathrm{a}+H_\mathrm{r}+H_\mathrm{ar},\rho]. \tag{22}$$

In order to obtain expressions for the lifetime and level shift, we need an equation of motion, a master equation, for the reduced atomic density operator ρ_a, defined by

$$\rho_\mathrm{a}(t)=\mathrm{Tr}_\mathrm{r}\rho(t). \tag{23}$$

Here the trace runs over the states of the radiation field only. With either reservoir theory [39] or the Zwanzig projection operator technique [40], we obtain

$$\frac{\mathrm{d}\rho_\mathrm{a}}{\mathrm{d}t}=-i(\omega_\mathrm{o}+\Delta)[|\mathrm{e}\rangle\langle\mathrm{e}|,\rho_\mathrm{a}] -\tfrac{1}{2}A\{|\mathrm{e}\rangle\langle\mathrm{e}|\rho_\mathrm{a}+\rho_\mathrm{a}|\mathrm{e}\rangle\langle\mathrm{e}|-2|\mathrm{g}\rangle\langle\mathrm{e}|\rho_\mathrm{a}|\mathrm{e}\rangle\langle\mathrm{g}|\}, \tag{24}$$

containing the Einstein A coefficient and the line shift Δ. the expressions for A and Δ will be given in Section 7. Eq. (24) governs the temporal evolution of the atomic density operator, and with the quantum regression theorem (or equivalent) this also yields atomic time-correlation functions. These, in turn, determine line shapes of the atomic transition, like the absorption profile given by Eq. (2). Furthermore, if we indicate by n_e the population of the excited state, which is $\langle e|\rho_a(t)|e\rangle$, then it follows immediately from Eq. (24) that

$$\frac{dn_e}{dt} = -An_e, \tag{25}$$

and for an atom initially in the excited state the solution is $n_e(t)=\exp(-At)$, e.g., exponential decay with a lifetime of $1/A$.

6. Correlation functions

From general relaxation theory, it follows that the rate constants and level shifts in the master equation (A and Δ here) can be expressed in terms of the Fourier–Laplace transforms of the field correlation functions at the position of the atom, defined by

$$g_{mn}(\omega)=\frac{1}{\hbar^2}\int_0^\infty d\tau\, e^{i\omega\tau}\langle A(\mathbf{r}_o,\tau)_m A(\mathbf{r}_o,0)_n\rangle,$$

$$m,n=x,y,\text{ or } z. \tag{26}$$

From the spatial symmetry of the configuration it can be shown that $g_{mn}(\omega)=0$ for $m\neq n$ and that $g_{xx}(\omega)=g_{yy}(\omega)$ [41]. Therefore, there are only two different nonzero correlation functions, which we shall denote as $g_\perp(\omega)=g_{zz}(\omega)$ and $g_\parallel(\omega)=g_{xx}(\omega)$.

The functions $g_\alpha(\omega)$, with $\alpha=\perp$ or $\parallel$, can be evaluated with the explicit expression (8) for the vector potential. The result has a different form depending on whether ω is positive or negative. We shall need $g_\alpha(\omega)$ for $\omega=\omega_o$ and $\omega=-\omega_o$, and these can be written in the form (at zero temperature)

$$g_\alpha(\omega_o)=\frac{\omega_o}{6\pi\epsilon_o\hbar c^3}b_\alpha(\omega_o) - \frac{i}{6\pi^2\epsilon_o\hbar c^3}P\int_0^\infty d\omega\,\frac{\omega}{\omega-\omega_o}b_\alpha(\omega), \tag{27}$$

$$g_\alpha(-\omega_o)=-\frac{i}{6\pi^2\epsilon_o\hbar c^3}\int_0^\infty d\omega\,\frac{\omega}{\omega+\omega_o}b_\alpha(\omega). \tag{28}$$

The P in Eq. (27) stands for principal value. The functions $b_\alpha(\omega)$ are given by

$$b_\perp(\omega)=\frac{3}{4}\int_0^1 du(1-u^2)\{|1+R_p\,e^{i\beta u}|^2+|T_p|^2\}, \tag{29}$$

$$b_\parallel(\omega)=\frac{3}{8}\int_0^1 du\{|1+R_s\,e^{i\beta u}|^2+|T_s|^2 + u^2|1-R_p\,e^{i\beta u}|^2+u^2|T_p|^2\}. \tag{30}$$

Here, u is again the cosine of the angle of incidence, and we have defined parameter β as

$$\beta=\frac{2\omega h}{c}, \tag{31}$$

which is a measure for the distance between the atom and the surface of the medium. The functions $b_\alpha(\omega)$, defined for $\omega>0$ only, are real and positive, and determined by the Fresnel coefficients (and β).

For ϵ real, we can use relation (19) to eliminate the transmission coefficients. It will be convenient to write the $b_\alpha(\omega)$'s as

$$b_\alpha(\omega)=1+c_\alpha(\omega), \tag{32}$$

which then gives

$$c_\perp(\omega)=\frac{3}{2}\,\mathrm{Re}\int_0^1 du(1-u^2)R_p\,e^{i\beta u}, \tag{33}$$

$$c_\parallel(\omega)=\frac{3}{4}\,\mathrm{Re}\int_0^1 du(R_s-u^2R_p)e^{i\beta u}. \tag{34}$$

These parameter functions depend on ω through the parameter β and the ω dependence of the Fresnel coefficients. Furthermore, they depend on ϵ, the layer thickness and the atom–surface distance h. Due to the integration over u we have

$$\lim_{h\to\infty} c_\alpha(\omega)=0, \tag{35}$$

because the fast oscillations of $\exp(i\beta u)$ average out to zero. This reflects the fact that when the

atom is far away from the surface, the medium has no influence any more on the properties of the atom.

7. Linewidth and line shift

For simplicity of notation we shall assume that the transition dipole moment matrix element $\boldsymbol{\mu}_{eg}$ is either perpendicular or parallel to the surface $z=0$. Then the Einstein A coefficient is determined by the field correlation according to

$$A=2\omega_o^2\boldsymbol{\mu}_{eg}\cdot\boldsymbol{\mu}_{eg}^*\mathrm{Re}\,g_\alpha(\omega_o), \tag{36}$$

where α now refers to the orientation of the atomic dipole. If we indicate by Δ_e and Δ_g the shifts of the excited state and ground state, respectively, then these level shifts are

$$\Delta_e=\omega_o^2\boldsymbol{\mu}_{eg}\cdot\boldsymbol{\mu}_{eg}^*\mathrm{Im}\,g_\alpha(\omega_o), \tag{37}$$

$$\Delta_g=\omega_o^2\boldsymbol{\mu}_{eg}\cdot\boldsymbol{\mu}_{eg}^*\mathrm{Im}\,g_\alpha(-\omega_o), \tag{38}$$

and the line shift is $\Delta=\Delta_e-\Delta_g$. In terms of the dimensionless parameter functions, we can write A as

$$A=A_o b_\alpha(\omega_o), \tag{39}$$

with A_o the free-space value from Eq. (1). This shows that $b_\alpha(\omega_o)$ is the correction factor for the Einstein A coefficient, representing the presence of the medium. Similarly, the line shift becomes

$$\Delta=\Delta_o+A_o J_\alpha, \tag{40}$$

where Δ_o is the free-space shift, formally given by

$$\Delta_o=A_o\frac{1}{\pi}P\int_0^\infty \mathrm{d}x\,\frac{x}{1-x^2}. \tag{41}$$

The integration variable is $x=\omega/\omega_o$. This integral diverges logarithmically in the upper limit. The correct value of this Lamb shift requires relativistic effects to be taken into account at the high frequency side. The effect of the medium is an additional (finite) shift A_oJ_α, with

$$J_\alpha=\frac{1}{\pi}P\int_0^\infty \mathrm{d}x\,\frac{x}{1-x^2}\,c_\alpha(x\omega_o), \tag{42}$$

the shift in units of the free-space Einstein A coefficient.

8. Linewidth near a metal

The dielectric constant ϵ of a metal is negative for visible light. This makes v from Eq. (18) positive imaginary for all u. In addition, we take the layer thickness much larger than a wavelength ($\ell\gg1$). With Eqs. (15) and (16) we then have $T_\sigma\to0$, $\sigma=s,\,p$, and as most easily seen from Eq. (19) this gives $|R_\sigma|=1$. Therefore, R_σ is a phase factor, and we write

$$R_\sigma=\mathrm{e}^{-2i\phi_\sigma}. \tag{43}$$

From Eqs. (13) and (14), we then find the phase angles to be

$$\phi_s=\arctan\left(\frac{\sqrt{1-\epsilon-u^2}}{u}\right), \tag{44}$$

$$\phi_p=\pi+\arctan\left(\frac{\sqrt{1-\epsilon-u^2}}{u\epsilon}\right). \tag{45}$$

With Eq. (43), expressions (33) and (34) for the $c_\alpha(\omega)$'s can be simplified somewhat.

An interesting limit is the theoretical perfect conductor (mirror) for which $\epsilon\to-\infty$. We then have $\phi_s\to\pi/2$, $\phi_p\to\pi$, $R_s\to-1$ and $R_p\to1$. The sign difference here is a consequence of the phase convention for the polarization vectors. With this simplification, the integrals in Eqs. (33) and (34) can be performed analytically, which yields

$$c_\perp(\omega)=-3\left\{\frac{\cos\beta}{\beta^2}-\frac{\sin\beta}{\beta^3}\right\}. \tag{46}$$

$$c_\parallel(\omega)=-\frac{3}{2}\left\{\frac{\sin\beta}{\beta}+\frac{\cos\beta}{\beta^2}-\frac{\sin\beta}{\beta^3}\right\}, \tag{47}$$

results that have been obtained many times and in many ways. The linewidths (in units of A_o) then are $b_\alpha=1+c_\alpha$, and with $\omega=\omega_o$. For the corresponding β we write β_o. In case of an atom close to the surface ($\beta\to0$), we have

$$b_\perp=2+\frac{1}{10}\beta^2+\ldots,\quad b_\parallel=-\frac{1}{5}\beta^2+\ldots, \tag{48}$$

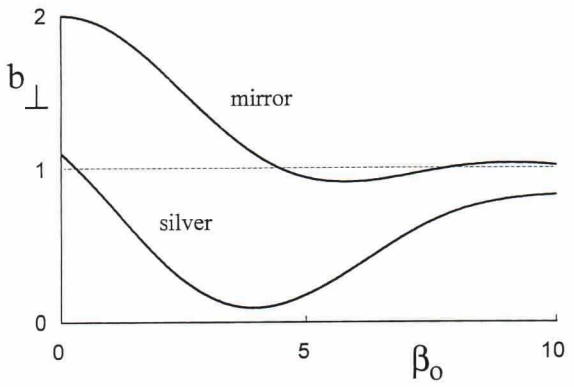

Fig. 2. Linewidth for a perpendicular dipole as a function of the (normalized) distance between the atom and the surface. From Eq. (31) it follows that β_0 equals 4π times the atom–surface distance, measured in units of a wavelength.

e.g., for a perpendicular dipole the linewidth is twice the natural width and for a parallel dipole the linewidth goes to zero. These features can be made plausible if one regards the system as a dipole and its mirror image.

One might wonder how realistic the limit of a perfect conductor is for the problem under consideration. According to Eq. (43), the reflectivity for any metal is unity, and the various vacuum waves only undergo a phase shift upon reflection. The best conductor, silver, has a dielectric constant of -15 (yellow light). Figs. 2 and 3 show the linewidths for silver, and the corresponding perfect conductor approximations from Eqs. (46) and (47), as a function of the distance between the atom and the surface. It is clear from Fig. 2 that the mirror limit is not a good approximation at all for a perpendicular dipole. In particular, for short distances the mirror results predicts a doubling of the linewidth [Eq. (48)], whereas for silver the linewidth is nearly equal to the natural width ($b_\perp \approx 1$). For a parallel dipole, on the other hand, Fig. 3 shows that the correspondence is reasonable. The fact that the mirror approximation is not necessarily adequate for this problem is because the superposition of plane waves in Eq. (8) for the vector potential is very phase sensitive. A finite ϵ gives finite phase shifts $2\phi_s$ and $2\phi_p$, and this can lead to either constructive or destructive interference of vacuum waves.

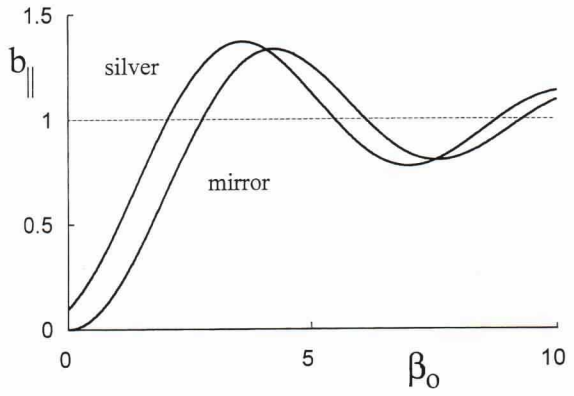

Fig. 3. Linewidth for a parallel dipole as a function of β_0 for silver and a perfect conductor.

9. Limit of a semi-infinite medium

The dependence on the layer thickness ℓ comes in through the Fresnel coefficients. For $u^2<1-\epsilon$ the parameter v is positive imaginary, and the factors $\exp(iv\ell)$ go to zero quickly for $\ell \gg 1$. This gives $R_\sigma \to \exp(-2i\phi_\sigma)$ and $T_\sigma \to 0$, as in the previous section. In general, this occurs for $\epsilon<0$, and for a part of the integration range over u for $0<\epsilon<1$ in the expressions (33) and (34) for the parameter functions. In this case the Fresnel coefficients R_s and R_p can alternatively be written as

$$R_s = \frac{u-v}{u+v}, \tag{49}$$

$$R_p = \frac{u\epsilon - v}{u\epsilon + v}, \tag{50}$$

and $T_\sigma = 0$.

On the other hand, when $u^2>1-\epsilon$, we have $|\exp(iv\ell)|=1$ for all ℓ, and these exponential factors keep on oscillating as a function of ℓ. This happens when $\epsilon>1$, and for a part of the integration range in the case $0<\epsilon<1$. In classical optics one then assumes that ϵ has a small positive imaginary part, giving v a small positive imaginary part, and then the Fresnel coefficients go again to the limits (49) and (50), with $T_\sigma=0$. The approach to this limit will be very slow, but for ℓ sufficiently large, this

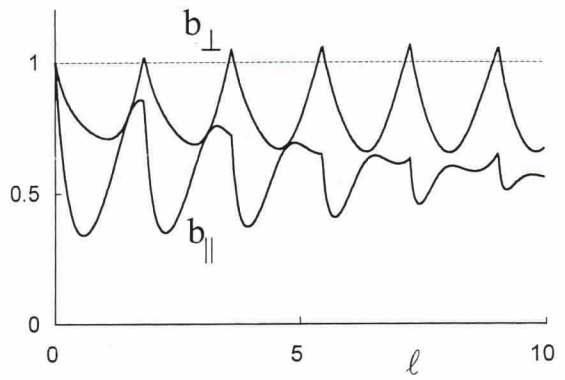

Fig. 4. Linewidth for a perpendicular and a parallel dipole as a function of the layer thickness (ℓ equals 2π times the thickness, measured in units of a wavelength), and for $\epsilon=4$, $\beta_0=1$.

limit would be reached eventually. For the present problem, however, this procedure leads to inconsistencies. When v is real, or real with a small imaginary part, we have $|R_\sigma|\neq 1$, and in combination with $T_\sigma=0$ this violates condition (19). It is then easy to see from Eqs. (29) and (30) that for such a situation the functions $b_\alpha(\omega)$ do not go to unity for $\beta\to\infty$, corresponding to an atom far away from the medium. This would be unphysical, and in violation of causality.

The oscillatory behavior of the linewidth as a function of ℓ is illustrated in Fig. 4. In Fig. 5 the same graph is extended to much higher ℓ values, and it appears that it levels off to a limit. The linewidth does not only oscillate rapidly as a function of ℓ, but for ℓ large, it also fluctuates fast as a function of ϵ. This feature is illustrated in Fig. 6. The reason is that ℓ enters through the factors $\exp[2i\ell(\epsilon-1+u^2)^{1/2}]$; for large ℓ, a small variation in ϵ leads to a large change in the exponent, and thereby to oscillatory behavior of the linewidth.

The question is then whether these oscillations are persistent for larger and larger ℓ, or that a true limit will be reached. The Fresnel coefficients keep on oscillating, and do not reach such a limit. The linewidth and the level shift, however, do have a limit for $\ell\to\infty$, as we will now show. In expressions (33) and (34) for the c_α's, the Fresnel coefficients are integrated over, with u as integration variable. The factors $\exp[2i\ell(\epsilon-1+u^2)^{1/2}]$ also vary rapidly as a function of u, and it can be expected that for ℓ very large these oscillations are smoothened out by the integration. The integrals appear in the form

$$\int_0^1 \mathrm{d}u\, R_\sigma\, \mathrm{e}^{i\beta u}, \tag{51}$$

or with an additional factor of u^2 in the integrand. Let us consider s-polarization, and introduce the variable $z=2\ell v$. Then R_s from Eq. (13) is

$$R_s=(1-\epsilon)\,\frac{1-\mathrm{e}^{iz}}{(v+u)^2-(v-u)^2\,\mathrm{e}^{iz}}, \tag{52}$$

where both v and z depend on the integration

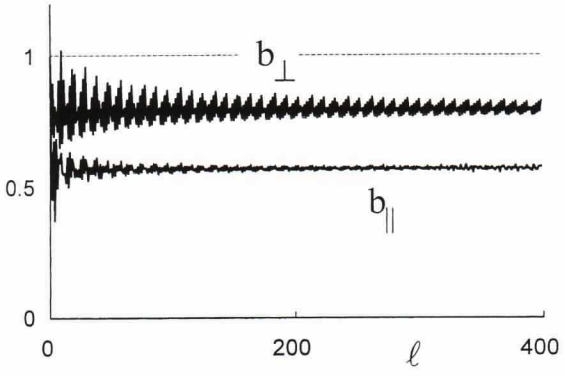

Fig. 5. Same as Fig. 4, but now extended to large values of ℓ. The seemingly chaotic behavior is due to numerical inaccuracies. In order to avoid extremely large computation times, we made each curve with only 400 points. The fast oscillations seen in Fig. 4 cannot be resolved in this way or on this scale.

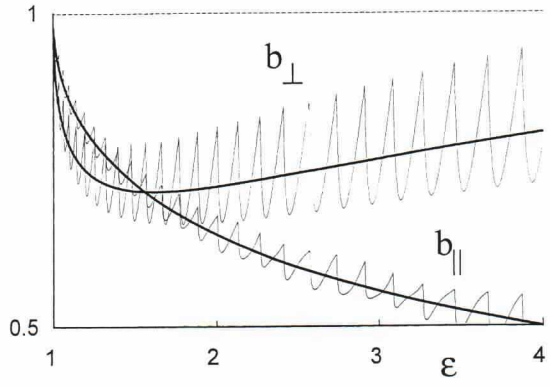

Fig. 6. The thin lines are the linewidths as a function of ϵ for $\beta=0$ and $\ell=50$. The oscillations are due to the large value of ℓ. The smooth thick lines are the values for $\ell\to\infty$.

variable u. For a small integration step over u from u_o to $u_o+\Delta u$, the only possible variation of the integrand comes from the factors $\exp(iz)$ in R_s. Therefore, for Δu small, we can write

$$\int_{u_o}^{u_o+\Delta u} du\, R_s\, e^{i\beta u} \approx e^{i\beta u_o} \int_{u_o}^{u_o+\Delta u} du\, R_s(u_o, z). \tag{53}$$

Here we have written $R_s=R_s(u, z)$, and we see this Fresnel coefficient as a function of two variables, as indicated by Eq. (52), and with $v=v(u)$. Then we make a change of integration variable from u to $z=2\ell(\epsilon-1+u^2)^{1/2}$, which gives

$$\int_{u_o}^{u_o+\Delta u} du\, R_s\, e^{i\beta u} \approx e^{i\beta u_o} \frac{\Delta u}{\Delta z} \int_{z_o}^{z_o+\Delta z} dz\, R_s\,(u_o, z). \tag{54}$$

Since $R_s(u_o, z)$ is periodic in z, with period 2π, we take $\Delta z=2\pi$. This makes the integral independent of z_o. The Fresnel coefficients averaged over a cycle, are defined by

$$\bar{R}_\sigma(u)=\frac{1}{2\pi}\int_0^{2\pi} dz\, R_\sigma(u, z), \tag{55}$$

by means of which we then have

$$\int_{u_o}^{u_o+\Delta u} du\, R_s\, e^{i\beta u} \approx e^{i\beta u_o} \Delta u\, \bar{R}_s(u_o). \tag{56}$$

In the limit $l\to\infty$ we have $\Delta u\to 0$, and this approximation becomes an identity. Summing over all Δu then yields

$$\int_0^1 du\, R_s\, e^{i\beta u} = \int_0^1 du\, \bar{R}_s(u) e^{i\beta u}, \tag{57}$$

and similarly for the integrals with R_p and u^2R_p. In conclusion, the limit $\ell\to\infty$ for the c_α's from Eqs. (33) and (34) follows from the substitution $R_\sigma\to\bar{R}_\sigma$, with the two $\bar{R}_\sigma$'s defined by Eq. (55).

In order to calculate $\bar{R}_s$ we first write R_s from Eq. (52) in the form

$$R_s=(1-\epsilon)\frac{2(v^2+u^2)(1-\cos z)-4ivu\sin z}{2(\epsilon-1)^2(1-\cos z)+(4vu)^2}. \tag{58}$$

With integrated from 0 to 2π, the term with $\sin(z)$ in the numerator gives no contribution, since this function is odd around $z=\pi$. The remaining integral has the form

$$\frac{1}{2\pi}\int_0^{2\pi} dz\, \frac{1-\cos z}{a-b\cos z}=\frac{1}{b}\left\{1-\sqrt{\frac{a-b}{a+b}}\right\}, \tag{59}$$

with $a>b>0$. Combining everything then yields the simple result

$$\bar{R}_s=\frac{u-v}{u+v}, \tag{60}$$

and a similar calculation gives for p-polarization

$$\bar{R}_p=\frac{u\epsilon-v}{u\epsilon+v}. \tag{61}$$

We then notice that Eqs. (60) and (61) are identical in form to Eqs. (49) and (50), pertaining to the case of v imaginary. Therefore we conclude that for the limit $\ell\to\infty$ we can replace R_s and R_p by $\bar{R}_s$ and $\bar{R}_p$, respectively, for all ϵ. Another interesting observation is the following. If we had allowed ϵ to have an imaginary part, then this damping would have a given exactly the same expressions for $\ell\to\infty$ as Eqs. (60) and (61). However, such a damping would also give $T_\sigma\to 0$, and this would violate relation (19). So, in the limit $\ell\to\infty$ the effective result for the reflection coefficients is the same as one would obtain by including damping, but without damping the t-waves do *not* disappear in general. They only do not show up explicitly anymore, because we have eliminated the T_σ coefficients with the help of Eq. (19).

Fig. 6 shows an example of the linewidths as a function of ϵ, for both ℓ finite and ℓ infinite. We have verified numerically that for increasing ℓ the oscillations get smaller indeed, and that the graph converges to the limit derived above. Similar conclusions hold for the linewidths as a function of β. Finally, the approach to the semi-infinite medium limit appears slow, and it might take up to $\ell\sim 10^3-10^4$ before this limit is reached within drawing accuracy for a graph. However, ℓ is the layer thickness measured in optical wavelengths and therefore a value of ℓ of the order of 10^3 still only corresponds to a layer thinner than a millime-

ter. From a macroscopic point of view, therefore, a thin layer can already be considered 'semi-infinite' in the sense of the limit discussed above.

10. Atom close to the surface

It does not appear possible to evaluate the integrals in Eqs. (33) and (34) explicitly, not even in the limit $\ell\to\infty$. The exception is the interesting case of $\beta\to 0$, corresponding to the situation where the atom is very close to the surface (compared to a wavelength radiation). When we substitute the $\bar{R}_\sigma$'s from Eqs. (60) and (61) into Eqs. (33) and (34) and use expression (18) for v, then the resulting integrals can be evaluated analytically. The only remaining parameter is the dielectric constant ϵ. The explicit formulas are given in Appendix A, and Fig. 7 shows the result. For a perfect conductor, $\epsilon\to-\infty$, we have $b_\perp\to 2$ and $b_\parallel\to 0$ [Eq. (48)], and we see from Fig. 7 that the approach to this limit is very slow, in particular for the parallel case. At the other side, $\epsilon\to\infty$, we also have $b_\perp\to 2$ and $b_\parallel\to 0$, and also that is not obvious from the graph or the formulas in Appendix A. It follows more directly from the fact that in this limit we have $\bar{R}_s\to -1$ and $\bar{R}_p\to 1$, which is the same as for a perfect conductor. The figure also verifies that for $\epsilon=1$ we have $b_\alpha=1$, as it must be for a pure transparent medium. For $\epsilon=0$ we find $b_\perp=0$ and $b_\parallel=1$, and for $\epsilon=-1$ we have $b_\perp=1/5$ and $b_\parallel=3/5$. For all ϵ shown in the graph, the linewidth is below the natural linewidth (unity), and this corresponds to an enhancement of the lifetime of the excited level. Only for large values of $|\epsilon|$ does $b_\perp$ become larger than unity. Numerically this was found to occur for $|\epsilon|>11.5$.

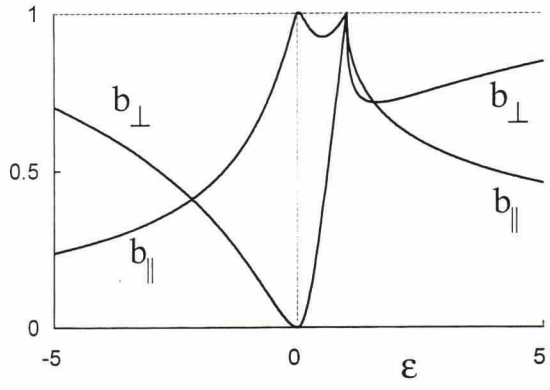

Fig. 7. Linewidths as a function of ϵ for the case of an atom close to the surface.

11. Line shift

The shift or the absorption line, $A_o J_\alpha$, is also determined by the parameter functions c_α, and is given by Eq. (42). The integral runs over all frequencies, where $x=\omega/\omega_o$. The frequency dependence of the c_α's is through the Fresnel coefficients and the factor $\exp(i\beta u)$. First, the layer thickness parameter ℓ depends on the frequency ω [Eq. (17)]. We shall consider again the limit of a semi-infinite medium, so that this ω-dependence disappears. The second ω-dependence is through the intrinsic frequency dependence of the dielectric constant. We shall assume that ϵ varies not too much over the range of interest, although this is not necessarily a good approximation. The only frequency dependence left in the integrand of J_α is then via the dimensionless atom–surface distance parameter β [(Eq. (31)]. We shall write $\beta=x\beta_o$, with $\beta_o=2\omega_o h/c$, as before. For $J_\perp$ we then obtain

$$J_\perp=\frac{3}{2\pi}\,\mathrm{Re}\,P\int_0^\infty dx\int_0^1 du\,\frac{x}{1-x^2}\,(1-u^2)\bar{R}_p\,e^{ix\beta_o u}. \tag{62}$$

Next we change the order of integration, and set $y=u\beta_o$. This yields

$$J_\perp=\frac{3}{2\pi\beta_o^3}\,\mathrm{Re}\int_0^{\beta_o} dy(\beta_o^2-y^2)\bar{R}_p\,Q(y), \tag{63}$$

where we have introduced the universal function $Q(y)$, defined as

$$Q(y)=P\int_0^\infty dx\,\frac{x}{1-x^2}\,e^{ixy},\quad y>0. \tag{64}$$

Similarly, $J_\parallel$ is

$$J_\parallel=\frac{3}{4\pi\beta_o^3}\,\mathrm{Re}\int_0^{\beta_o} dy(\beta_o^2\bar{R}_s-y^2\bar{R}_p)Q(y). \tag{65}$$

The advantage of integrating over x first is that the function $Q(y)$ can be evaluated in terms of elementary functions. After factoring the denominator and splitting the integrand into its real and imaginary part, we obtain

$$Q(y)=\cos y\,\mathrm{Ci}\,y+\sin y\,\mathrm{Si}\,y-\frac{i\pi}{2}\cos y, \tag{66}$$

in terms of the cosine and sine integrals $\mathrm{Ci}(y)$ and $\mathrm{Si}(y)$, respectively. With the known properties of these functions [42], we can transform the definition (64) into the alternative form

$$Q(y)=\left(\gamma-\frac{i\pi}{2}+\ln y\right)\cos y-\int_0^y \mathrm{d}t\,\frac{\cos t-\cos y}{t-y}, \tag{67}$$

with $\gamma=0.577216$, Euler's constant. From either form we can derive the values of $Q(y)$ for y small and large,

$$Q(y)=\gamma+\ln y-\frac{i\pi}{2}+\ldots,\quad y\downarrow 0, \tag{68}$$

$$Q(y)\approx-\frac{i\pi}{2}\,\mathrm{e}^{iy},\quad y\to\infty, \tag{69}$$

showing that the real part has a logarithmic singularity at $y=0$. The graph of this parameter-free function is presented in Fig. 8. Functions $\mathrm{Ci}y$ and $\mathrm{Si}y$ are obtained from a standard routine [43].

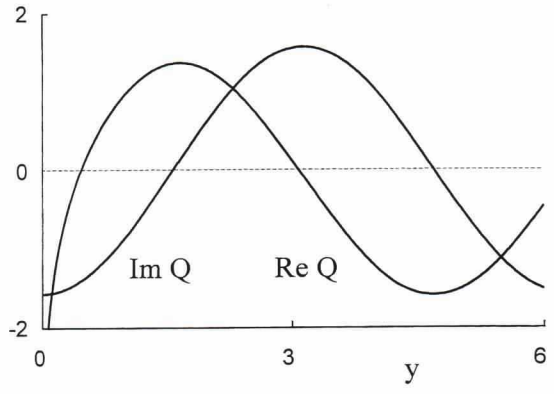

Fig. 8. Graph of the real and imaginary part of the function $Q(y)$.

The integrals in Eqs. (63) and (64) have to be evaluated numerically, but part of the integration can still be done analytically. In particular, the logarithmic singularity of $Q(y)$ for $y\downarrow 0$ poses no problems. We introduce two auxiliary functions:

$$f(y)=\int \mathrm{d}y\,Q(y), \tag{70}$$

$$g(y)=\int \mathrm{d}y\,y^2 Q(y), \tag{71}$$

which can be computed with some effort. The result is

$$f(y)=\sin y\,\mathrm{Ci}\,y-\cos y\,\mathrm{Si}\,y-\frac{i\pi}{2}\sin y, \tag{72}$$

$$g(y)=y^2 f(y)+2y(\cos y\,\mathrm{Ci}\,y+\sin y\,\mathrm{Si}\,y-1)+2\cos y\,\mathrm{Si}\,y-2\sin y\,\mathrm{Ci}\,y+i\pi(\sin y-y\cos y), \tag{73}$$

for $y>0$. For $y\downarrow 0$, this gives $f(0)=g(0)=0$. The function $Q(y)$ oscillates approximately with a period of 2π. The integrations run from $y=0$ to $y=\beta_o$, and for β_o large this runs over many oscillations. On the other hand, the Fresnel coefficients vary only slowly over the integration interval. We therefore divide the integration interval in N steps, such that the Fresnel coefficients do not vary significantly over each step. In the examples below, we took $N=100$. Then it does not matter how the function $Q(y)$ varies, because with Eqs. (72) and (73) this integration is done exact. In particular, the first step from $y=0$, which involves the logarithmic singularity of $Q(y)$, is integrated correctly. In this fashion, we get for instance

$$\int_0^{\beta_o}\mathrm{d}y\,y^2\bar{R}_p(u)Q(y)\approx\sum_{i=1}^{N}\bar{R}_p(u_i)[g(y_i)-g(y_{i-1})], \tag{74}$$

with $u_i=y_i/\beta_o$.

The limit of a perfect conductor now follows easily. Then we have $\bar{R}_s=-1$ and $\bar{R}_p=1$, indepen-

dent of u. We then immediately obtain

$$J_\perp = \frac{3}{2\pi\beta_o^3}\,\mathrm{Re}\{\beta_o^2 f(\beta_o) - g(\beta_o)\}, \tag{75}$$

$$J_\parallel = \frac{-3}{4\pi\beta_o^3}\,\mathrm{Re}\{\beta_o^2 f(\beta_o) + g(\beta_o)\}, \tag{76}$$

and with Eqs. (72) and (73) these can be expressed in terms of cosine and sine integrals. For β_o large these lines shifts are

$$J_\perp = \frac{3}{\pi\beta_o^2}\left\{1 - \frac{\pi}{2}\sin\beta_o + \mathcal{O}\left(\frac{1}{\beta_o}\right)\right\}, \tag{77}$$

$$J_\parallel = \frac{3}{4\beta_o}\cos\beta_o\left\{1 + \mathcal{O}\left(\frac{1}{\beta_o}\right)\right\}. \tag{78}$$

Similarly, for small β_o we obtain

$$J_\perp \approx \frac{1}{\pi}\left\{\gamma - \frac{4}{3} + \ln\beta_o\right\}, \tag{79}$$

$$J_\parallel \approx -\frac{1}{\pi}\left\{\gamma - \frac{5}{6} + \ln\beta_o\right\}, \tag{80}$$

showing that $J_\perp$ is negative, whereas $J_\parallel$ is positive.

Figs. 9 and 10 compare the line shifts for a mirror with the results for silver. As in Figs. 2 and 3, we find again that for a parallel dipole the agreement is very good, but in the perpendicular case the perfect conductor approximation is not great. Fig. 11 illustrates the behavior of the line shifts a as a function β_o for a dielectric material. In this case, both $J_\perp$ and $J_\parallel$ go to $+\infty$ for β_o small. For $\beta_o \to 0$, the line shifts always diverge. In Fig. 12 we graph the line shifts for β_o small for a range of the dielectric constant. We notice that the shifts are predominantly positive, except for a perpendicular dipole in the extreme cases of a perfect conductor or ϵ very large. It can be shown in general that the behavior for β_o small is given by

$$J_\alpha \approx \frac{1}{\pi}\,c_\alpha \ln\beta_o + \text{constant}, \tag{81}$$

as a generalization of Eqs. (79) and (80). Here, c_α is evaluated at $\beta_o = 0$. Therefore, the sign of J_α is the opposite of the sign of c_α.

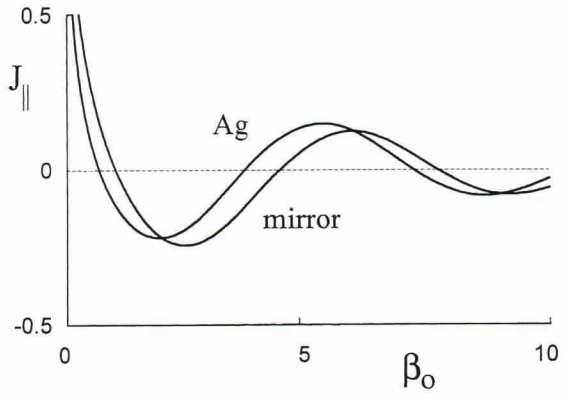

Fig. 10. Same as Fig. 9, but now for a parallel dipole.

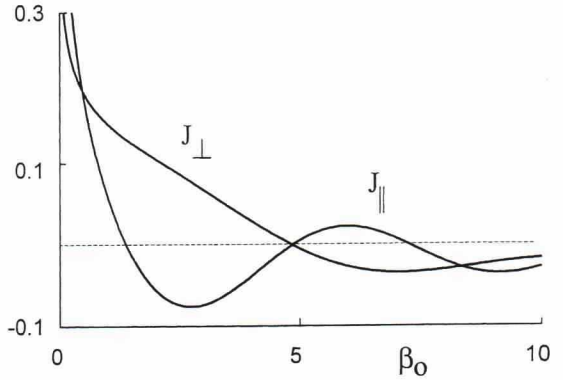

Fig. 11. Line shifts as a function of β_o for $\epsilon = 4$.

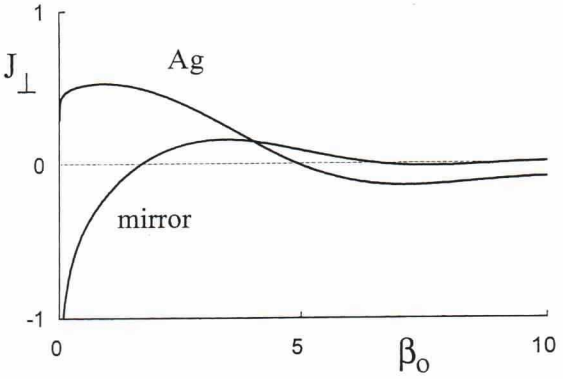

Fig. 9. Line shift as a function of the atom–surface distance for silver and for a mirror, for the situation of a perpendicular dipole moment. Both curves go to $-\infty$ for $\beta_o \to 0$, although that is not clear on this scale for silver.

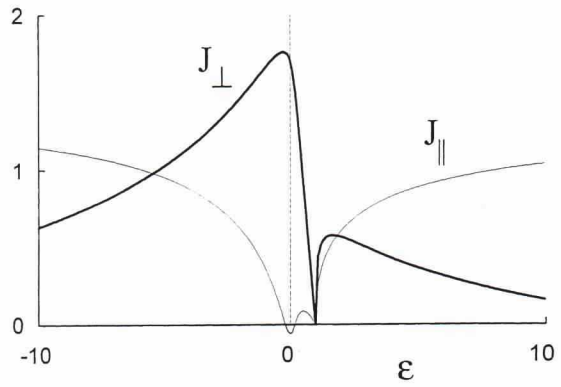

Fig. 12. Line shifts for $\beta_o=0.01$ as a function of ϵ. Around $\epsilon=0$, the $J_\parallel$ dips slightly below zero, but apart from that, the shifts appear to be positive. Extension of the graph to higher and lower values of ϵ shows that $J_\perp$ eventually becomes negative for $|\epsilon|$ large, as was the case for a perfect conductor in the limit of small β_o.

12. Conclusions

We have studied the linewidth and line shift of a model two-level atomic transition near a layer of dielectric material, as these result from the coupling of the atomic dipole moment to the radiative part in the electromagnetic vacuum near such a medium. In particular, we consider how the limit of a semi-infinite medium is reached. It turned out that the usual approach of including a small imaginary part in the dielectric constant, to provide damping, does not apply in general in quantum mechanics. For $\epsilon<0$, both ways yield the same result, but for $\epsilon>0$ there is a difference. The existence of a limit is the result of an effective averaging over fast oscillations due to the integration over the angle of incidence of the vacuum field waves. For $\epsilon>0$, the t-waves, which originate below the medium, do not vanish on average, whereas in the approach with $Im\,\epsilon>0$, these waves would also damp out.

It turned out that for an atom close to the material, the integrals representing the linewidths could be obtained analytically (the results are given in Appendix A and shown graphically in Fig. 7). We have developed an, at least numerically, attractive method to calculate the line shift integrals. These are principal value integrals over a singularity at $x=1$, and running up to $x=\infty$. With our method, this problem is dealt with analytically by means of the $Q(y)$ function. This $Q(y)$ can be expressed as an integral over a finite interval and without a singularity [Eq. (67)], or in terms of elementary functions [Eq. (66)]. With the help of the functions $f(y)$ and $g(y)$, Eqs. (72) and (73), we can then evaluate the line shifts easily. The behavior of the linewidths and line shifts as a function of the various parameters was illustrated, and in particular it was found that a metal is not approximated very well by a perfect conductor in the case of a perpendicular dipole.

Appendix A

The parameter functions $c_\perp$ and $c_\parallel$ from Eqs. (33) and (34), respectively, can be evaluated analytically for $\beta=0$ and $\ell\to\infty$. For the Fresnel coefficients we have to use Eqs. (60) and (61), with v given by Eq. (18). This v can be positive ($\epsilon>1$) or positive imaginary ($\epsilon<0$). It has a branch point at $u=(1-\epsilon)^{1/2}$, and for $0<\epsilon<1$ this is in the integration interval [0, 1]. We have verified graphically that the expressions below give the same results as numerical integration.

For $\epsilon<-1$:

$$c_\perp=\frac{1}{\epsilon^2-1}\left\{\epsilon^2+1-\frac{3\epsilon^2}{\epsilon+1}\times\left[1+\frac{\epsilon}{\sqrt{-\epsilon-1}}\arctan\left(\sqrt{-\epsilon-1}\right)\right]\right\},\quad\text{(A1)}$$

$$c_\parallel=-\frac{1}{2}\frac{\epsilon}{\epsilon^2-1}\left\{2\epsilon+1+\frac{3\epsilon}{\epsilon+1}\times\left[1-\frac{1}{\sqrt{-\epsilon-1}}\arctan\left(\sqrt{-\epsilon-1}\right)\right]\right\}.\quad\text{(A2)}$$

For $-1<\epsilon<0$:

$$c_\perp=\frac{1}{\epsilon^2-1}\left\{\epsilon^2+1-\frac{3\epsilon^2}{\epsilon+1}\times\left[1+\frac{\epsilon}{\sqrt{\epsilon+1}}\operatorname{arctanh}\left(\sqrt{\epsilon+1}\right)\right]\right\},\quad\text{(A3)}$$

$$c_{\parallel}=-\frac{1}{2}\frac{\epsilon}{\epsilon^2-1}\left\{2\epsilon+1+\frac{3\epsilon}{\epsilon+1}\times\left[1-\frac{1}{\sqrt{\epsilon+1}}\operatorname{arctanh}\left(\sqrt{\epsilon+1}\right)\right]\right\}. \tag{A4}$$

For $0<\epsilon<1$:

$$c_{\perp}=-\frac{1}{16}\frac{(\epsilon-1)^2}{\epsilon+1}\left[\sqrt{1-\epsilon}-\frac{(1+\sqrt{\epsilon})^2}{1-\sqrt{\epsilon}}\right]-\frac{1}{16}(\epsilon+1)\left[\sqrt{1-\epsilon}-\frac{(1-\sqrt{\epsilon})^2}{1+\sqrt{\epsilon}}\right]+\frac{3}{4(\epsilon^2-1)(\epsilon+1)}\left\{2\left[\epsilon^3-\epsilon^2+\epsilon+1\right]+\epsilon^{3/2}(\epsilon^2-4\epsilon-1)+\frac{1}{2}(\epsilon^4-1)\left(1+\frac{1}{3}\sqrt{1-\epsilon}\right)-\frac{8\epsilon^3}{\sqrt{\epsilon+1}}\operatorname{arctanh}\left(\frac{1-\sqrt{3}}{\sqrt{\epsilon+1}}\right)\right\}, \tag{A5}$$

$$c_{\parallel}=-\frac{1}{32}\frac{(\epsilon-1)^2}{\epsilon+1}\left[\sqrt{\epsilon-1}-\frac{(1+\sqrt{\epsilon})^2}{1-\sqrt{\epsilon}}\right]-\frac{1}{32}(\epsilon+1)\left[\sqrt{1-\epsilon}-\frac{(1-\sqrt{\epsilon})^2}{1+\sqrt{\epsilon}}\right]+\frac{1}{4(\epsilon-1)}(2\epsilon^{3/2}+1-3\epsilon)+\frac{3}{8(\epsilon^2-1)(\epsilon+1)}\times\left\{\epsilon^{3/2}(\epsilon^2+3)-4\epsilon^2+\frac{1}{2}(\epsilon^4-1)\left(1+\frac{1}{3}\sqrt{1-\epsilon}\right)+\frac{8\epsilon^2}{\sqrt{\epsilon+1}}\operatorname{arctanh}\left(\frac{1-\sqrt{3}}{\sqrt{\epsilon+1}}\right)\right\}. \tag{A6}$$

For $\epsilon>1$:

$$c_{\perp}=\frac{1}{16}\frac{(\epsilon-1)^2}{\epsilon+1}\left[\sqrt{\epsilon-1}+\frac{(1+\sqrt{\epsilon})^2}{1-\sqrt{\epsilon}}\right]-\frac{1}{16}(\epsilon+1)\left[\sqrt{\epsilon-1}-\frac{(1-\sqrt{\epsilon})^2}{1+\sqrt{\epsilon}}\right]+\frac{3}{4(\epsilon^2-1)(\epsilon+1)}\left\{2\left[\epsilon^3-\epsilon^2+\epsilon+1\right]+\epsilon(\sqrt{\epsilon}-\sqrt{\epsilon-1})(\epsilon^2-4\epsilon-1)+\frac{1}{2}(\epsilon^4-1)-\frac{8\epsilon^3}{\sqrt{\epsilon+1}}\left[\operatorname{arctanh}\left(\frac{1-\sqrt{\epsilon}}{\sqrt{\epsilon+1}}\right)-\frac{1}{2}\ln\left(\epsilon-\sqrt{\epsilon^2-1}\right)\right]\right\}, \tag{A7}$$

$$c_{\parallel}=\frac{1}{32}\frac{(\epsilon-1)^2}{\epsilon+1}\left[\sqrt{\epsilon-1}+\frac{(1+\sqrt{\epsilon})^2}{1-\sqrt{\epsilon}}\right]-\frac{1}{32}(\epsilon+1)\left[\sqrt{\epsilon-1}-\frac{(1-\sqrt{\epsilon})^2}{1+\sqrt{\epsilon}}\right]+\frac{1}{4(\epsilon-1)}\left\{2\left(\epsilon^{3/2}-(\epsilon-1)^{3/2}\right)+1-3\epsilon\right\}+\frac{3}{8(\epsilon^2-1)(\epsilon+1)}\times\left\{\epsilon(\sqrt{\epsilon}-\sqrt{\epsilon-1})(\epsilon^2+3)-4\epsilon^2+\frac{1}{2}(\epsilon^4-1)+\frac{8\epsilon^2}{\sqrt{\epsilon+1}}\left[\operatorname{arctanh}\left(\frac{1-\sqrt{\epsilon}}{\sqrt{\epsilon+1}}\right)-\frac{1}{2}\ln\left(\epsilon-\sqrt{\epsilon^2-1}\right)\right]\right\}. \tag{A8}$$

References

[1] E.M. Purcell, Phys. Rev. 69 (1946) 681.
[2] W. Heitler, The Quantum Theory of Radiation, third ed., Dover, New York, 1984. chapter 5.
[3] R. Loudon, The Quantum Theory of Light, second ed., Clarendon, Oxford, 1983, p. 179.
[4] K.H. Drexhage, in: E. Wolf (Ed.), Progress in Optics XII, North-Holland Amsterdam, 1974, p. 165.
[5] R.R. Chance, A. Prock, R. Silbey, J. Chem. Phys. 60 (1974) 2744.
[6] R.R. Chance, A.H. Miller, A. Prock, R. Silbey, Chem. Phys. Lett. 33 (1975) 590.
[7] R.R. Chance, A.H. Miller, A. Prock, R. Silbey, J. Chem. Phys. 63 (1975) 1589.
[8] R.R. Chance, A. Prock, R. Silbey, Adv. Chem. Phys. 39 (1978) 1.
[9] P. Goy, J.M. Raimond, M. Gross, S. Haroche, Phys. Rev. Lett. 50 (1983) 1903.

[10] R.G. Hulet, E.S. Hilfer, D. Kleppner, Phys. Rev. Lett. 55 (1985) 2137.
[11] F. De Martini, G. Innocenti, G.R. Jacobovitz, P. Mataloni, Phys. Rev. Lett. 59 (1987) 2955.
[12] W. Jhe, A. Anderson, E.A. Hinds, D. Meschede, L. Moi, S. Haroche, Phys. Rev. Lett. 58 (1987) 666.
[13] D.J. Heinzen, J.J. Childs, J.E. Thomas, M.S. Feld, Phys. Rev. Lett. 58 (1987) 1320.
[14] E. Snoeks, A. Lagendijk, A. Polman, Phys. Rev. Lett. 74 (1995) 2459.
[15] H. Morawitz, Phys. Rev. 187 (1969) 1792.
[16] P.W. Milonni, P.L. Knight, Opt. Commun. 9 (1973) 119.
[17] D. Meschede, W. Jhe, E.A. Hinds, Phys. Rev. A 41 (1990) 1587.
[18] R.R. Chance, A. Prock, R. Silbey, J. Chem. Phys. 62 (1975) 2245.
[19] R.R. Chance, A. Prock, R. Silbey, J. Chem. Phys. 65 (1976) 2527.
[20] J.E. Sipe, Surf. Sci. 105 (1981) 489.
[21] G.S. Agarwal, Phys. Rev. Lett. 32 (1974) 703.
[22] G.S. Agarwal, Phys. Rev. A 12 (1975) 1475.
[23] J.M. Wylie, J.E. Sipe, Phys. Rev. A 30 (1984) 1185.
[24] D.J. Heinzen, M.S. Feld, Phys.Rev. Lett. 59 (1987) 2623.
[25] P.W. Milonni, The Quantum Vacuum, Academic Press, Boston, 1993. p. 82.
[26] G. Barton, Proc. R. Soc. Lond. A 320 (1970) 251.
[27] G. Barton, J. Phys. B 7 (1974) 2134.
[28] R.R. Chance, A. Prock, R. Silbey, Phys. Rev. A 12 (1975) 1448.
[29] J.M. Wilie, J.E. Sipe, Phys. Rev. A 32 (1985) 2030.
[30] W. Jhe, Phys. Rev. A 43 (1991) 5795.
[31] W. Jhe, Phys. Rev. A 44 (1991) 5932.
[32] C. Cohen-Tannoudji, J. Dupont-Roc, G. Grynberg, Photons and Atoms, Wiley, New York, 1989. p. 304.
[33] J.J. Sakurai, Modern Quantum Mechanics, revised ed., Addison-Wesley, Reading, MA, 1994. p. 338.
[34] C.M. Caves, Phys. Rev. D 26 (1982) 1817.
[35] A.L. Gaeta, R.W. Boyd, Phys. Rev. Lett. 60 (1988) 2618.
[36] C. Cohen-Tannoudji, in: G. Grynberg, R. Stora (Eds.), New Trends in Atomic Physics, Proc. of the XXXVIIIth Les Houches Summer School of Theoretical Physics, North-Holland, Amsterdam, 1984, p. 5.
[37] M. Born, E. Wolf, Principles of Optics, sixth ed., Pergamon, Oxford, 1980, p. 61.
[38] R.M.A. Azzam, N.M. Bashara, Ellipsometry and Polarized Light, North-Holland, Amsterdam, 1987. p. 283.
[39] W.H. Louisell, Quantum Statistical Properties of Radiation, Wiley, New York, 1973. chapter 6.
[40] G.S. Agarwal, Quantum Optics, Springer Tracts in Modern Physics vol. 70, Springer, Berlin, 1974.
[41] H.F. Arnoldus, T.F. George, Surf. Sci. 205 (1988) 617.
[42] M. Abramowitz, I.A. Stegun, Handbook of Mathematical Functions, Dover, New York, 1970. p. 231.
[43] W.H. Press, S.A. Teukolsky, W.T. Vetterling, B.P. Flannery, Numerical Recipes in Fortran 77 vol. 1, Cambridge, New York, 1992, p. 248.